Available online at www.sciencedirect.com
SCIENCE DIRECT
C. R. Mecanique 333 (2005) 636–641
COMPTES RENDUS MECANIQUE
http://france.elsevier.com/direct/CRAS2B/

Thermocapillary motion of a two-bubble cluster near a plane solid wall

Antoine Sellier

LadHyX, École polytechnique, 91128 Palaiseau cedex, France

Received 17 February 2005; accepted after revision 22 June 2005

Available online 8 August 2005

Presented by Sébastien Candel

Abstract

The thermocapillary motion of two bubbles near a plane solid wall at uniform temperature is investigated by solving five boundary integral-equations. Preliminary computations show that wall–bubble interactions dictate the migration of equal bubbles with line of centers parallel to the wall. ***To cite this article: A. Sellier, C. R. Mecanique 333 (2005).***

Résumé

Sur la migration thermocapillaire d'une paire de bulles en présence d'une paroi plane rigide. Le mouvement thermocapillaire de deux bulles au voisinage d'un plan solide isotherme est obtenu par résolution de cinq équations intégrales de frontière. Les calculs présentés montrent que les interactions paroi–bulle pilotent en première approximation le mouvement de deux bulles de mêmes rayons placées à des distances identiques du plan. ***Pour citer cet article : A. Sellier, C. R. Mecanique 333 (2005).***

Keywords: Fluid mechanics; Thermocapillarity; Wall–bubble interactions; Bubble–bubble interactions; Boundary formulation

Mots-clés : Mécanique des fluides ; Thermocapillarité ; Interactions bulle–paroi ; Interactions bulle–bulle ; Formulation intégrale

1. Introduction

A single spherical bubble with radius a and temperature-dependent surface tension $\gamma(T)$ of constant slope $\gamma' = \mathrm{d}\gamma/\mathrm{d}T$ migrates [1] when freely suspended in a Newtonian fluid of uniform viscosity μ and subject to a uniform temperature gradient ∇T_∞ at the velocity $\mathbf{U} = -a\gamma'\nabla T_\infty/[2\mu]$. This velocity is affected in presence of other bubbles or boundaries and pure bubble–bubble and wall–bubble interactions have been thus investigated for

E-mail address: sellier@ladhyx.polytechnique.fr (A. Sellier).

1631-0721/$ – see front matter
doi:10.1016/j.crme.2005.06.010

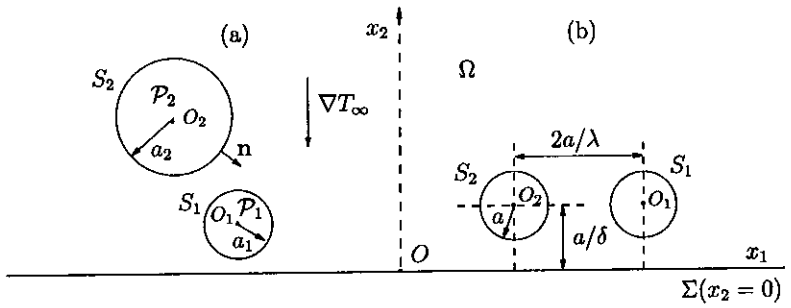

Fig. 1. A two-bubble cluster near the hot ($\nabla T_\infty \cdot \mathbf{e}_2 < 0$) $x_2 = 0$ plane solid wall Σ: (a) an arbitrary cluster with $\mathbf{O_1O_2} \cdot \mathbf{e}_3 = 0$; (b) the case of two equal bubbles ($a = a_1 = a_2$) with $\mathbf{O_1O_2} \wedge \mathbf{e}_1 = \mathbf{0}$.

Fig. 1. Paire de bulles au voisinage d'un plan solide Σ ($x_2 = 0$) chaud ($\nabla T_\infty \cdot \mathbf{e}_2 < 0$) : (a) cas d'une configuration arbitraire avec $\mathbf{O_1O_2} \cdot \mathbf{e}_3 = 0$; (b) cas de deux bulles identiques ($a = a_1 = a_2$) telles que $\mathbf{O_1O_2} \wedge \mathbf{e}_1 = \mathbf{0}$.

several bubbles in absence of boundary [2–5] and one bubble near a plane wall [6–8]. In addition, [9] addresses combined wall–bubble and bubble–bubble interactions for two equal bubbles assumed to move parallel to a very close wall. This work deals with the general case of a 2-bubble cluster in the vicinity of a plane solid wall at uniform temperature, i.e. when the velocity of each bubble is allowed to be non-tangent to the wall.

2. Advocated boundary-integral approach

We adopt Cartesian coordinates (O, x_1, x_2, x_3) with $\mathbf{x} = \mathbf{OM}$, $x_k = \mathbf{x} \cdot \mathbf{e}_k$ (see Fig. 1(a)) and consider two spherical bubbles $\mathcal{P}_n$ ($n = 1, 2$) with center O_n, radius a_n and surface S_n, freely suspended in a Newtonian liquid of uniform viscosity μ above the $x_2 = 0$ plane solid wall Σ and subject to a uniform ambient temperature gradient ∇T_∞ normal to Σ.

The non-conducting surface S_n has normal $\mathbf{n} = \mathbf{O_nM}/a_n$ and temperature-dependent surface tension γ_n with $\gamma_n' = \mathrm{d}\gamma_n/\mathrm{d}T$ uniform. The bubble $\mathcal{P}_n$ translates, with respect to Σ, at the unknown velocity $\mathbf{U}^{(n)}$ and the liquid experiences in the fluid domain Ω velocity, pressure and disturbed temperature fields $\mathbf{u}$, p and $T_\infty + T'$, respectively. For vanishing Reynolds and Marangoni numbers, T' and the flow $(\mathbf{u}, p)$ with stress tensor $\boldsymbol{\sigma}$ obey [6]

$$\nabla^2 T' = \nabla \cdot \mathbf{u} = 0 \quad \text{and} \quad \mu \nabla^2 \mathbf{u} = \nabla p \quad \text{in } \Omega; \quad (\nabla T', \mathbf{u}, p) \to (\mathbf{0}, \mathbf{0}, 0) \quad \text{as } |\mathbf{OM}| \to \infty \tag{1}$$

$$\nabla T' \cdot \mathbf{n} = -\nabla T_\infty \cdot \mathbf{n}, \quad \mathbf{u} \cdot \mathbf{n} = \mathbf{U}^{(n)} \cdot \mathbf{n}, \quad \boldsymbol{\sigma} \cdot \mathbf{n} - [\mathbf{n} \cdot \boldsymbol{\sigma} \cdot \mathbf{n}]\mathbf{n} = -\gamma_n' \nabla [T_\infty + T'] \quad \text{on } S_n \tag{2}$$

$$\mathbf{u} = \mathbf{0} \quad \text{and} \quad T' = 0 \quad \text{on } \Sigma, \qquad \int_{S_n} \boldsymbol{\sigma} \cdot \mathbf{n} \, \mathrm{d}S = \mathbf{0} \quad \text{for } n = 1, 2 \tag{3}$$

Note that $\nabla [T_\infty + T'] \wedge \mathbf{n} = \mathbf{0}$ on each S_n whereas the integral conditions in (3) hold because the bubbles are freely suspended. Setting $U_k^{(n)} = \mathbf{U}^{(n)} \cdot \mathbf{e}_k$ and selecting $\mathbf{O_1O_2} \cdot \mathbf{e}_3 = 0$ yields $U_3^{(1)} = U_3^{(2)} = 0$ for symmetry reasons. Mimicking [4], we introduce for $n = 1, 2$ and $i = 1, 2$ four Stokes flows $(\mathbf{u}_i^{(n)}, p_i^{(n)})$ with stress tensor $\boldsymbol{\sigma}_i^{(n)}$ subject to (1) and the conditions

$$\mathbf{u}_i^{(n)} = \mathbf{0} \quad \text{on } \Sigma, \quad \boldsymbol{\sigma}_i^{(n)} \cdot \mathbf{n} = \left[\mathbf{n} \cdot \boldsymbol{\sigma}_i^{(n)} \cdot \mathbf{n}\right]\mathbf{n} \quad \text{and} \quad \mathbf{u}_i^{(n)} \cdot \mathbf{n} = \delta_{nm} \mathbf{e}_i \cdot \mathbf{n} \quad \text{on } S_m \tag{4}$$

with δ_{nm} the Kronecker Delta, and (for n, m, i and j in $\{1, 2\}$) the associated coefficients

$$A_{ij}^{(n),(m)} = \int_{S_m} (\mathbf{e}_j \cdot \mathbf{n})(\mathbf{n} \cdot \boldsymbol{\sigma}_i^{(n)} \cdot \mathbf{n}) \, \mathrm{d}S \tag{5}$$

Extending the treatment advocated in [4], (1)–(3) then yield for the unknown generalized velocity $X = (U_1^{(1)}, U_2^{(1)}, U_1^{(2)}, U_2^{(2)})$ the following key linear 4-equation system

$$\sum_{m=1}^{2}\sum_{j=1}^{2} A_{ij}^{(n),(m)} U_j^{(m)} = \sum_{m=1}^{2} \int_{S_m} \gamma_m' \left(\delta_{nm}\mathbf{e}_i - \mathbf{u}_i^{(n)}\right) \cdot \nabla[T_\infty + T'] \,\mathrm{d}S, \quad n = 1,2;\ i = 1,2 \tag{6}$$

The system (6) has a real-valued, symmetric and negative-definite matrix (for conciseness the proof is omitted) and therefore admits a unique solution X readily obtained by solely evaluating $\nabla[T_\infty + T']$, $\mathbf{u}_i^{(n)}$ and $\mathbf{n}\cdot\boldsymbol{\sigma}_i^{(n)}\cdot\mathbf{n}$ on $S = S_1 \cup S_2$. In order to calculate such quantities we first use the second Green identity for T' governed by (1)–(3). Denoting by $\mathbf{x}'(x_1, -x_2, x_3)$ the symmetric of a point $\mathbf{x}(x_1, x_2, x_3)$ in Ω with respect to Σ one thus easily obtains the following boundary-integral equation of the second kind

$$\begin{aligned} -4\pi T'(\mathbf{x}) &+ \int_{S\setminus S_m} T'(\mathbf{y}) \frac{(\mathbf{x}-\mathbf{y})\cdot\mathbf{n}(\mathbf{y})}{|\mathbf{x}-\mathbf{y}|^3}\,\mathrm{d}S(\mathbf{y}) + \int_{S_m} \left[T'(\mathbf{y}) - T'(\mathbf{x})\right] \frac{(\mathbf{x}-\mathbf{y})\cdot\mathbf{n}(\mathbf{y})}{|\mathbf{x}-\mathbf{y}|^3}\,\mathrm{d}S(\mathbf{y}) \\ &- \int_S T'(\mathbf{y}) \frac{(\mathbf{x}'-\mathbf{y})\cdot\mathbf{n}(\mathbf{y})}{|\mathbf{x}'-\mathbf{y}|^3}\,\mathrm{d}S(\mathbf{y}) = \int_S [\nabla T_\infty\cdot\mathbf{n}](\mathbf{y}) \left[\frac{1}{|\mathbf{x}'-\mathbf{y}|} - \frac{1}{|\mathbf{x}-\mathbf{y}|}\right] \mathrm{d}S(\mathbf{y}) \quad \text{for } \mathbf{x} \text{ on } S_m \end{aligned} \tag{7}$$

Inverting (7) provides T' on S and the vector $\nabla[T_\infty + T']$ is evaluated on each S_m by computing there the tangential derivatives of $T_\infty + T'$. For any pair (n, i) we also look on S, where $d = \mathbf{u}_i^{(n)}\cdot\mathbf{n}$ is given, at $a = \mathbf{n}\cdot\boldsymbol{\sigma}_i^{(n)}\cdot\mathbf{n}/\mu$ and the tangential velocity $\mathbf{a} = \mathbf{u}_i^{(n)} - d\mathbf{n}$. Adopting henceforth the tensor summation convention for indices k, l and p in $\{1,2,3\}$, the Green tensor $\mathbf{G}'(\mathbf{y},\mathbf{x}) = G'_{kl}(\mathbf{y},\mathbf{x})\mathbf{e}_k\otimes\mathbf{e}_l$ vanishing on Σ (i.e. $G'_{kl}(\mathbf{y},\mathbf{x}) = 0$ for $\mathbf{y}\cdot\mathbf{e}_2 = 0$) and the associated stress tensor $\mathbf{T}'(\mathbf{y},\mathbf{x}) = T'_{klp}(\mathbf{y},\mathbf{x})\mathbf{e}_k\otimes\mathbf{e}_l\otimes\mathbf{e}_p$ are given by [10]

$$\begin{aligned} G'_{kl}(\mathbf{y},\mathbf{x}) = {} & \frac{\delta_{kl}}{|\mathbf{x}-\mathbf{y}|} + \frac{[(\mathbf{x}-\mathbf{y})\cdot\mathbf{e}_k][(\mathbf{x}-\mathbf{y})\cdot\mathbf{e}_l]}{|\mathbf{x}-\mathbf{y}|^3} - \left\{\frac{\delta_{kl}}{|\mathbf{x}'-\mathbf{y}|} + \frac{[(\mathbf{x}'-\mathbf{y})\cdot\mathbf{e}_k][(\mathbf{x}'-\mathbf{y})\cdot\mathbf{e}_l]}{|\mathbf{x}'-\mathbf{y}|^3}\right\} \\ & - \frac{2c_l(\mathbf{x}\cdot\mathbf{e}_2)}{|\mathbf{x}'-\mathbf{y}|^3}\left\{\delta_{k2}(\mathbf{x}'-\mathbf{y})\cdot\mathbf{e}_l - \delta_{l2}(\mathbf{x}'-\mathbf{y})\cdot\mathbf{e}_k + (\mathbf{y}\cdot\mathbf{e}_2)\left[\delta_{kl} - \frac{3[(\mathbf{x}'-\mathbf{y})\cdot\mathbf{e}_k][(\mathbf{x}'-\mathbf{y})\cdot\mathbf{e}_l]}{|\mathbf{x}'-\mathbf{y}|^2}\right]\right\} \end{aligned} \tag{8}$$

$$\begin{aligned} T'_{klq}(\mathbf{y},\mathbf{x}) = {} & \frac{6[(\mathbf{x}-\mathbf{y})\cdot\mathbf{e}_k][(\mathbf{x}-\mathbf{y})\cdot\mathbf{e}_l][(\mathbf{x}-\mathbf{y})\cdot\mathbf{e}_q]}{|\mathbf{x}-\mathbf{y}|^5} - \frac{6[(\mathbf{x}'-\mathbf{y})\cdot\mathbf{e}_k][(\mathbf{x}'-\mathbf{y})\cdot\mathbf{e}_l][(\mathbf{x}'-\mathbf{y})\cdot\mathbf{e}_q]}{|\mathbf{x}'-\mathbf{y}|^5} \\ & - \frac{12c_l(\mathbf{x}\cdot\mathbf{e}_2)}{|\mathbf{x}'-\mathbf{y}|^5}\left\{\delta_{kq}\left[(\mathbf{x}'-\mathbf{y})\cdot\mathbf{e}_l\right]\left[(\mathbf{x}'-\mathbf{y})\cdot\mathbf{e}_2\right] - \delta_{l2}\left[(\mathbf{x}'-\mathbf{y})\cdot\mathbf{e}_k\right]\left[(\mathbf{x}'-\mathbf{y})\cdot\mathbf{e}_q\right]\right. \\ & - (\mathbf{y}\cdot\mathbf{e}_2)\left(\delta_{kq}\left[(\mathbf{x}'-\mathbf{y})\cdot\mathbf{e}_l\right] + \delta_{kl}\left[(\mathbf{x}'-\mathbf{y})\cdot\mathbf{e}_q\right] + \delta_{lq}\left[(\mathbf{x}'-\mathbf{y})\cdot\mathbf{e}_k\right]\right. \\ & \left.\left. + \frac{5[(\mathbf{x}'-\mathbf{y})\cdot\mathbf{e}_k][(\mathbf{x}'-\mathbf{y})\cdot\mathbf{e}_l][(\mathbf{x}'-\mathbf{y})\cdot\mathbf{e}_q]}{|\mathbf{x}'-\mathbf{y}|^5}\right)\right\} \end{aligned} \tag{9}$$

with $c_1 = c_3 = 1$ and $c_2 = -1$. Using the material in [11], the property $\boldsymbol{\sigma}_i^{(n)}\wedge\mathbf{n} = \mathbf{0}$ on S and the conditions (4) then makes it possible to prove that a and $a_k = \mathbf{a}\cdot\mathbf{e}_k$ (for $k = 1,2,3$) obey the boundary-integral equation (with summations over indices k, l and p)

$$\begin{aligned} &\left\{8\pi a_l(\mathbf{x}) - \int_{S_m} \left[a_k(\mathbf{y}) - a_k(\mathbf{x})\right] T'_{klp}(\mathbf{y},\mathbf{x}) n_p(\mathbf{y})\,\mathrm{d}S(\mathbf{y}) - \int_{S\setminus S_m} a_k(\mathbf{y}) T'_{klp}(\mathbf{y},\mathbf{x}) n_p(\mathbf{y})\,\mathrm{d}S(\mathbf{y})\right. \\ &\left. + \int_S G'_{kl}(\mathbf{y},\mathbf{x}) n_k(\mathbf{y}) a(\mathbf{y})\,\mathrm{d}S(\mathbf{y})\right\}\mathbf{e}_l = \left\{-8\pi[dn_l](\mathbf{x}) + \int_{S\setminus S_m} [dn_k](\mathbf{y}) T'_{klp}(\mathbf{y},\mathbf{x}) n_p(\mathbf{y})\,\mathrm{d}S(\mathbf{y})\right. \\ &\left. + \int_{S_m} \left\{[dn_k](\mathbf{y}) - [dn_k](\mathbf{x})\right\} T'_{klp}(\mathbf{y},\mathbf{x}) n_p(\mathbf{y})\,\mathrm{d}S(\mathbf{y})\right\}\mathbf{e}_l \quad \text{for } \mathbf{x} \text{ on } S_m\ (m = 1,2) \end{aligned} \tag{10}$$

Table 1
Comparisons with [6] (for M if $\lambda = 0$) and [2] (for (M, N) if $\delta = 0$) using increasing numbers $N_1 = N_2$ of nodal points on each bubble. Here $\lambda_3 = 1/1.0811$

Tableau 1
Comparaisons pour M si $\lambda = 0$ avec [6] et pour (M, N) si $\delta = 0$ avec [2] en utilisant différents nombres $N_1 = N_2$ de points de collocation sur les bulles. Ici, $\lambda_3 = 1/1.0811$

(M, N)	(λ, δ)	$N_1 = 74$	$N_1 = 242$	$N_1 = 530$	$N_1 = 1058$	[6,2]
M	$(0, 0.2)$	0.9664	0.9909	0.9943	0.9947	0.9950
M	$(0, 2/3)$	0.7724	0.7914	0.7943	0.7945	0.7948
M	$(0, \lambda_3)$	0.3388	0.3197	0.3139	0.3139	0.3145
M	$(0.2, 0)$	0.9726	0.9965	0.9998	1.0002	1.0005
N	$(0.2, 0)$	−0.0002	−0.0005	−0.0005	−0.0005	−0.0005
M	$(0.6, 0)$	0.9852	1.0096	1.0130	1.0134	1.0137
N	$(0.6, 0)$	−0.0124	−0.0135	−0.0137	−0.0137	−0.0137
M	$(0.9, 0)$	1.0194	1.0441	1.0479	1.0483	1.0486
N	$(0.9, 0)$	−0.0464	−0.0485	−0.0485	−0.0486	−0.0486

In summary, the velocity $(U_1^{(1)}, U_2^{(1)}, U_1^{(2)}, U_2^{(2)})$ is gained from (6) by solving five boundary-integral equations: (7) and (10) for $n = 1, 2$ and $i = 1, 2$. As in [5], the numerical implementation uses 6-node isoparametric boundary elements on S with N_m nodes on S_m and the linear systems resulting from (7) and (10) are solved by Gaussian elimination.

3. Preliminary numerical results and discussion

This section presents numerical comparisons and new results for two equal bubbles ($a_1 = a_2 = a$) with $\gamma_n' < 0$, $\eta = \gamma_2'/\gamma_1'$ and $\mathbf{O_1O_2} \cdot \mathbf{e}_2 = 0$ (see Fig. 1(b)). This geometry is characterized by the positive wall–bubble and bubble–bubble separation parameters $\delta = a/\mathbf{OO_1} \cdot \mathbf{e}_2 < 1$ and $\lambda = 2a/O_1O_2 < 1$. In addition, by linearity and for symmetry reasons, the normalized velocities $\mathbf{v}^{(n)} = -2\mu\mathbf{U}^{(n)}/[\gamma_n' a_n \nabla T_\infty \cdot \mathbf{e}_2]$ can be written:

$$\mathbf{v}^{(1)} = [M' + \eta N']\mathbf{e}_1 + [M + \eta N]\mathbf{e}_2, \qquad \mathbf{v}^{(2)} = -[M' + N'/\eta]\mathbf{e}_1 + [M + N/\eta]\mathbf{e}_2 \tag{11}$$

with mobility coefficients M, N, M' and N' depending upon (λ, δ). For $\lambda\delta = 0$ bubbles move normal to Σ ($M' = N' = 0$) and the computed values of M for distant bubbles ($\lambda = 0$) and of (M, N) in absence of wall ($\delta = 0$) are compared with [6,2] for $N_1 = N_2$ nodal points in Table 1. Note that [6,2] resort to a quite different approach using bipolar coordinates.

Clearly, using 530-node meshes yields a nice accuracy of order of 0.1%. Accordingly, we select $N = 530$ when investigating combined wall–bubble and bubble–bubble interactions for $\delta\lambda \neq 0$. The computed coefficients M, N, M' and N' are plotted in Fig. 2.

As depicted in Fig. 2(a), M is positive, deeply sensitive to the wall position δ and much less sensitive to the bubble–bubble separation λ. Other coefficients N, M' and N' are small in magnitude compared to M, negligible for $\lambda \leqslant 0.2$ whatever δ and either positive or negative for $\lambda > 0.2$. Near the wall (for $\delta \geqslant 0.8$) M is nearly constant and M' and N' (not N) increase in magnitude with λ large enough. By virtue of (11) and Fig. 2(a) and (b), the velocities $v_2^{(n)} = \mathbf{v}^{(n)} \cdot \mathbf{e}_2$ are positive for $\eta = O(1)$. By contrast, since M' and N' of comparable magnitudes satisfy $M'N' < 0$ for δ large enough, as seen in Fig. 2(c) and (d), velocity components $v_1^{(n)} = \mathbf{v}^{(n)} \cdot \mathbf{e}_1$ will exhibit a more subtle behaviour versus (λ, δ) and η. We illustrate this feature for two identical bubbles ($a_2 = a_1$ and $\eta = \gamma_2'/\gamma_1' = 1$) in Fig. 3.

As expected, $v_2^{(1)} = v_2^{(2)}$ weakly depends on λ (wall–bubble interactions are dominant for the motion normal to Σ) and the velocity component $v_1^{(1)} = -v_1^{(2)}$ parallel to Σ deeply depends on (λ, δ): it is negative far enough

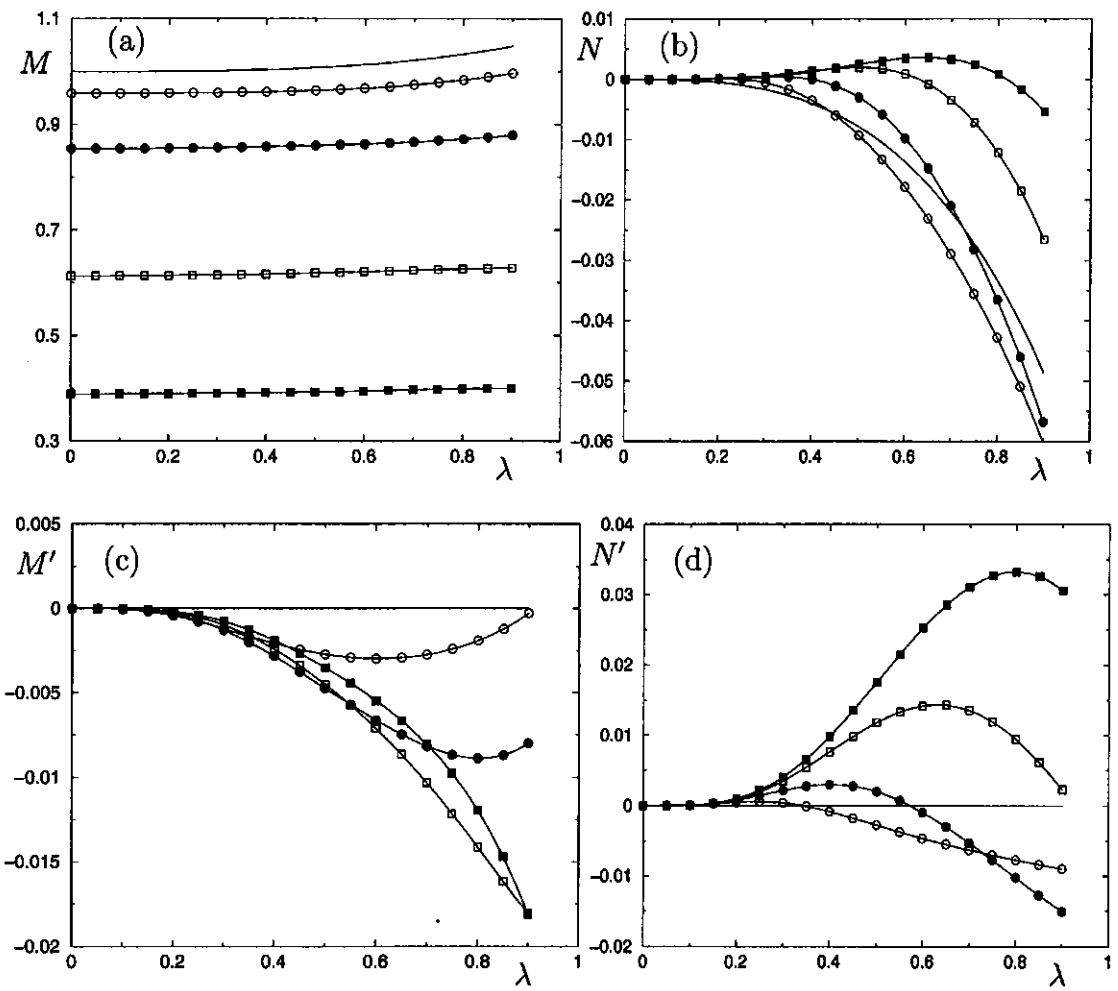

Fig. 2. Coefficients M, N, M' and N' for $\delta = 0$ (solid curves), $\delta = 0.4$ (○), $\delta = 0.6$ (●), $\delta = 0.8$ (□) and $\delta = 0.9$ (■). (a) M. (b) N. (c) M'. (d) N'.

Fig. 2. Coefficients M, N, M' et N' pour $\delta = 0$ (courbes en traits pleins), $\delta = 0.4$ (○), $\delta = 0.6$ (●), $\delta = 0.8$ (□) et $\delta = 0.9$ (■). (a) M. (b) N. (c) M'. (d) N'.

from Σ ($\delta = 0.4$), positive close enough to Σ ($\delta = 0.9$) and either zero at a critical spacing λ_c, positive for distant bubbles ($\lambda < \lambda_c$) and negative for close bubbles ($\lambda > \lambda_c$) if $\delta = 0.6$ or $\delta = 0.8$. For $\delta = 0.9$ the monotonic plot (dashed curve in Fig. 3(b)) of v_1, obtained as in [9], is due to quite different conditions: $U_2^{(n)} = 0$ and (only) $[\int_{S_n} \boldsymbol{\sigma} \cdot \mathbf{n}\, dS] \wedge \mathbf{e}_2 = \mathbf{0}$. Finally, note that two identical bubbles with $\delta \leqslant 0.4$ at initial time will successively separate each other and then approach as time evolves when moving toward a hot wall ($\nabla T_\infty \cdot \mathbf{e}_2 < 0$ with $\mathbf{O_1O_2} \cdot \mathbf{e}_2 = 0$). This behavior agrees with experiments [9].

4. Conclusions

For two equal bubbles ($a_1 = a_2$) with $\mathbf{O_1O_2} \cdot \mathbf{e}_2 = 0$ it is found that combined wall–bubble and bubble–bubble interactions induce a weak velocity component parallel to the wall and that for $\gamma_2' = O(\gamma_1')$ the migration is dictated

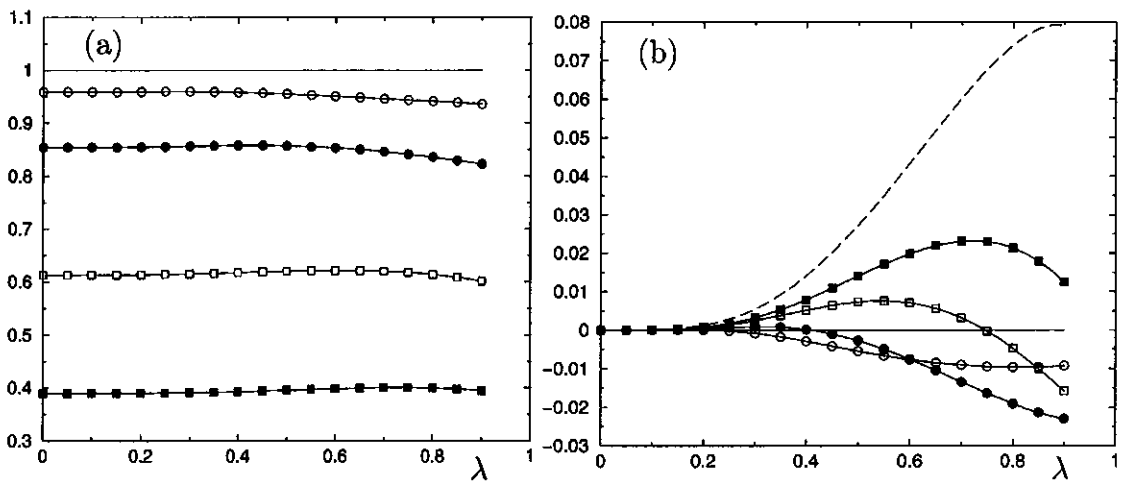

Fig. 3. Normalized velocities $v_i = \mathbf{v}_i^{(1)}$ for identical bubbles ($a_2 = a_1, \eta = 1$) with $i = 1, 2$ and $\delta = 0$ (solid curves), $\delta = 0.4$ (○), $\delta = 0.6$ (●), $\delta = 0.8$ (□), $\delta = 0.9$ (■). (a) v_2. (b) v_1 with results obtained as in [9] for $\delta = 0.9$ indicated by a long-dashed curve.

Fig. 3. Vitesses adimensionnées $v_i = \mathbf{v}_i^{(1)}$ pour des bulles identiques ($a_2 = a_1, \eta = 1$) si $i = 1, 2$ et $\delta = 0$ (solid curves), $\delta = 0.4$ (○), $\delta = 0.6$ (●), $\delta = 0.8$ (□), $\delta = 0.9$ (■). (a) v_2. (b) v_1 avec aussi pour $\delta = 0.9$ des résultats obtenus comme dans [9] et indiqués en traits pointillés.

by wall–bubble interactions: a bubble nearly moves as if alone near the wall. This latter property might however breakdown not only if $a_1 \neq a_2$ or $\mathbf{O}_1\mathbf{O}_2 \cdot \mathbf{e}_2 \neq 0$ but also when ∇T_∞ is parallel to the wall. Such cases are therefore under current analysis.

References

[1] N.O. Young, J.S. Goldstein, M.J. Block, The motion of bubbles in a vertical temperature gradient, J. Fluid Mech. 197 (1959) 350–356.
[2] H.J. Keh, L.S. Chen, Droplet interactions in thermocapillary migration, J. Chem. Engrg. Sci. 48 (1993) 3565–3582.
[3] Y. Wang, R. Maury, A. Acrivos, Thermocapillary migration of a bidisperse suspension of bubbles, J. Fluid Mech. 261 (1994) 47–64.
[4] A. Sellier, On the capillary motion of arbitrary clusters of spherical bubbles. Part 1. General theory, J. Fluid Mech. 197 (2004) 391–401.
[5] A. Sellier, On the slow motion of a cluster of bubbles under the combined action of gravity and thermocapillarity, C. R. Mecanique 333 (2) (2005) 111–116.
[6] M. Meyyapan, W.R. Wilcox, R.S. Subramanian, Thermocapillary migration of a bubble normal to a plane surface, J. Colloid Interface Sci. 83 (1981) 199–208.
[7] M. Meyyapan, R.S. Subramanian, Thermocapillary migration of a gas bubble in an arbitrary direction with respect to a plane surface, J. Colloid Interface Sci. 115 (1987) 206–219.
[8] H. Kasumi, Y.E. Solomentsev, S.A. Guelcher, J.L. Anderson, P.J. Sides, Thermocapillary flow and aggregation of bubbles on a solid wall, J. Colloid Interface Sci. 232 (2000) 111–120.
[9] H. Kasumi, P.J. Sides, J.L. Anderson, Interactions between two bubbles on a hot or cold wall, J. Colloid Interface Sci. 276 (2004) 239–247.
[10] J.R. Blake, A note on the image system for a Stokeslet in a no-slip boundary, Proc. Cambridge Philos. Soc. 70 (1971) 303–310.
[11] C. Pozrikidis, Boundary Integral and Singularity Methods for Linearized Viscous Flow, Cambridge University Press, Cambridge, 1992.